Dual-mechanism ERK1/2 inhibitors exploit a distinct binding mode to block phosphorylation and nuclear accumulation of ERK1/2

Andrew M Kidger[1*], Joanne M. Munck[2], Harpreet K. Saini[2], Kathryn Balmanno[1], Emma Minihane[1], Aurelie Courtin[2], Brent Graham[2], Marc O'Reilly[2], Richard Odle[1] & Simon J Cook[1*]

[1]Signalling Laboratory, The Babraham Institute, Babraham Research Campus, Cambridge CB22 3AT, UK

[2]Astex Pharmaceuticals, 436 Cambridge Science Park, Cambridge CB4 0QA, UK

*Correspondence to: Simon J Cook, Signalling Laboratory, The Babraham Institute, Babraham Research Campus, Cambridge, CB22 3AT, UK. Email: simon.cook@babraham.ac.uk

Andrew Kidger, Signalling Laboratory, The Babraham Institute, Babraham Research Campus, Cambridge, CB22 3AT, UK. Email: andrew.kidger@babraham.ac.uk

Running title

Dual-mechanism ERK1/2 inhibitors display increased potency

Keywords

ERK1/2, ERK inhibitors, MEK, RAF, RAS

Disclosure of Potential Conflicts of Interest

The authors declare the following competing interests: J.M.M., H.K.S., A.C., B.G. and M.O. are paid employees of Astex Pharmaceuticals. Some work in S.J.C.'s laboratory was supported by a sponsored research collaboration funded by Astex Pharmaceuticals and awarded through the Milner Therapeutics Consortium; this paid A.M.K.'s salary. S.J.C. served as a consultant for Astex Pharmaceuticals. All other authors declare no other competing interests.

Abstract

The RAS-regulated RAF-MEK1/2-ERK1/2 signalling pathway is frequently deregulated in cancer due to activating mutations of growth factor receptors, RAS or BRAF. Both RAF and MEK1/2 inhibitors are clinically approved and various ERK1/2 inhibitors (ERKi) are currently undergoing clinical trials. To date ERKi display two distinct mechanisms of action (MoA); catalytic ERKi solely inhibit ERK1/2 catalytic activity, whereas dual mechanism ERKi additionally prevent the activating phosphorylation of ERK1/2 at its T-E-Y motif by MEK1/2. These differences may impart significant differences in biological activity because T-E-Y phosphorylation is the signal for nuclear entry of ERK1/2, allowing them to access many key transcription factor targets. Here, we characterised the MoA of five ERKi and examined their functional consequences in terms of ERK1/2 signalling, gene expression and anti-proliferative efficacy. We demonstrate that catalytic ERKi promote a striking nuclear accumulation of p-ERK1/2 in KRAS mutant cell lines. In contrast, dual mechanism ERKi exploit a distinct binding mode to block ERK1/2 phosphorylation by MEK1/2, exhibit superior potency and prevent the nuclear accumulation of ERK1/2. Consequently, dual-mechanism ERKi exhibit more durable pathway inhibition and enhanced suppression of ERK1/2-dependent gene expression compared to catalytic ERKi, resulting in increased efficacy across BRAF and RAS mutant cell lines.

Introduction

The RAS-RAF-MEK1/2-ERK1/2 signalling pathway drives cell survival and proliferation (1). Activation of the RAS GTPases results in the dimerization and activation of RAF kinases (2,3), which then phosphorylate and activate MEK1/2, which subsequently phosphorylate threonine and tyrosine residues within the T-E-Y motif of the ERK1/2 activation loop. This promotes ERK1/2 activation and release from MEK1/2, enabling ERK1/2 to phosphorylate cytoplasmic substrates and promoting its nuclear translocation to phosphorylate transcription factors to regulate gene expression and drive cell cycle progression (1,4). The magnitude and duration of ERK1/2 activity is controlled by intrinsic negative feedback systems including the direct inhibitory phosphorylation of upstream pathway components (5) and the *de novo* expression of MAP kinase phosphatases (MKPs/DUSPs)(6) and the Sprouty proteins (7).

ERK1/2 signalling is frequently deregulated in cancer due to activating mutations in receptor tyrosine kinases (RTKs), RAS or BRAF, resulting in constitutive pathway activation (8) and small-molecule RAF and MEK1/2 inhibitors (RAFi, MEKi) are now approved and used in the clinic (9,10). Lessons from the use of RAFi and MEKi have prompted interest in targeting the pathway at the level of ERK1/2 for two reasons. First, innate resistance to RAFi or MEKi involves the relief of negative feedback, resulting in the restoration of ERK1/2 activity in the presence of drug, validating the use of ERK1/2 inhibitors (ERKi) in combination to target tumours that are refractory to RAFi or MEKi monotherapy (9,11). Second, acquired resistance to RAFi or MEKi emerges through mechanisms (KRAS or BRAF amplification, BRAF splice variants, MEK mutation) that re-instate ERK1/2 signalling, validating the use of ERKi to overcome or forestall acquired resistance to RAFi or MEKi (12–15).

The first selective ERKi are undergoing clinical evaluation and include: BVD-523 (ulixertinib) (16,17), GDC-0994 (18), LY-3214996 (19), MK-8353 (clinical derivative of SCH772984) (20,21), ASTX029 (22), LTT462 (23) and KO-947 (24). Furthermore, multiple pre-clinical compounds have been disclosed (25–31). The majority of these ERKi target ERK1/2 catalytic activity in a reversible, ATP-competitive manner (catalytic ERKi or catERKi). However, dual mechanism ERKi (dmERKi), including SCH772984 and Compound 27 (a potent and selective ERKi developed using fragment-based drug discovery) can additionally antagonise ERK1/2 T-E-Y phosphorylation by MEK1/2, preventing the formation of the active conformation of ERK1/2 (20,21,25). These distinct mechanisms of action (MoA) could have important consequences for how cells respond and adapt following ERKi treatment.

MEKi that inhibit both the phosphorylation of MEK1/2 by RAF and MEK1/2 catalytic activity are proposed to delay pathway rebound following feedback relief, causing a more durable inhibition of ERK1/2 and cell proliferation compared to purely catalytic MEKi (32–34). DmERKi act similarly to these “feedback buster” MEKi, so might also delay pathway rebound relative to catERKi. Furthermore, by inhibiting ERK1/2 T-E-Y phosphorylation by MEK1/2 dmERKi should inhibit ERK1/2 nuclear translocation; this could promote more robust suppression of ERK1/2-dependent gene expression relative to catERKi (11). In contrast, catERKi treatment may promote accumulation of p-ERK1/2 (16,21), which would be expected to drive its nuclear localisation. This could facilitate accelerated ERK1/2-dependent gene expression when compound efficacy is lost, resulting in cells recovering more rapidly from treatment with catERKi compared to dmERKi. Accumulation of nuclear p-ERK1/2 following catERKi treatment may also maintain the proposed kinase-independent functions of ERK1/2, including interactions with topoisomerase II (35), poly(ADP-ribose) polymerase (PARP) 1 (36) and DUSP6 (37). Furthermore, binding of nuclear ERK1/2 to lamin A can displace the retinoblastoma (RB) protein, facilitating RB phosphorylation by cyclin-dependent kinases, release of E2F transcription factors and cell cycle entry (38). Finally, ERK2 acts as a transcriptional repressor of interferon-responsive genes by directly binding DNA in their promoter regions (39). Most proposed

kinase-independent functions of ERK1/2 occur in the nucleus and could persist with nuclear accumulation of ERK1/2 following catERKi treatment. The impact of this on the relative efficacy of catERKis, dmERKis or MEK inhibitors that prevent ERK1/2 phosphorylation and nuclear import has not been addressed to date.

In this study, we characterised the binding mode and ability to modulate ERK1/2 phosphorylation and nuclear accumulation of five ERKi. We also examined their efficacy, their suppression of pathway rebound and effects on ERK1/2-dependent gene expression. We demonstrate that dmERKi exploit a distinct binding mode to block ERK1/2 phosphorylation by MEK1/2 and inhibit the nuclear translocation of ERK1/2. Consequently, dmERKi exhibit increased potency and an improved ability to delay pathway rebound in RAS mutant cell lines, resulting in a more robust suppression of ERK1/2 activity and ERK1/2-dependent gene expression compared to catERKi.

Materials and Methods

Reagents and Cell Lines

The source and RRID of all reagents and cell lines utilised are detailed in Table S1. Cells were grown in DMEM (CO115, DLD-1, HCT116, LoVo, A375), Leibovitz's L-15 (Sw480), McCoy's 5A (HT29), MEMα (RKO) or RPMI1640 (COLO205, SK-MEL-30) media supplemented with 10% (v/v) fetal bovine serum, penicillin (100U/mL), streptomycin (100mg/mL) and 2mM glutamine. Cells were incubated in a humidified incubator at 37°C and 5% (v/v) CO2. All cell lines were authenticated by Short Tandem Repeat (STR) profiling and confirmed negative for mycoplasma prior to experiments commencing. Experiments were performed within 2 months of thawing, except for the generation of drug-resistant cells lines for which the culture time is indicated in the respective figures.

In Vivo Studies

The care and treatment of experimental animals were in accordance with the United Kingdom Coordinating Committee for Cancer Research guidelines (40) and the United Kingdom Animals (Scientific Procedures) Act 1986 (41). Mouse studies were performed with mice allowed access to food and water *ad libitum*.

COLO205 xenografts were prepared by subcutaneously injecting 5×10^6 cells suspended in serum-free medium mixed 1:1 with Matrigel (BD Biosciences, USA) into the right flank of each male BALB/c nude mouse. A single dose of compound was administered orally to the mice. Tumors were excised and flash-frozen in liquid nitrogen at indicated time-points. Tumour lysates were prepared by grinding with a mortar/pestle under liquid nitrogen prior to addition of ice-cold lysis buffer (Meso Scale Discovery, Maryland, USA), and incubated at 4°C for 30 minutes.

SDS-PAGE and Western blotting

Cell lysis, SDS-PAGE and Western blotting were performed as previously described (42), with the modification to use fluorescently-tagged secondary antibodies to enable band visualisation and quantification on a Li-Cor Odyssey imaging system (LI-COR Biosciences, UK). Membranes were cut to allow probing for multiple molecular weight proteins. Where appropriate, blots were probed with different species of antibodies, using multiple colours to detect the same molecular weight on the same membrane. If necessary multiple independent blots were performed using the lysate from each experiment. Quantification of the protein of interest was normalised to an appropriate loading control. Antibodies are detailed in Table S1.

High content microscopy and analysis of EdU incorporation, p-ERK1/2, ERK1/2 and p-RSK levels

Immunofluorescence staining and high-content microscopy were performed as previously described (42,43), with reagents used detailed in Table S1. Briefly, cells were seeded in 96-well imaging plates (CellCarrier-96, Perkin Elmer, UK) and treated 24 hours later as indicated in the Figure legends. For EdU incorporation analysis, cells were incubated with 10μM EdU for the last hour of treatment, except in background control wells where no EdU was added. Cells were then harvested and fixed with 4% formaldehyde/PBS, washed once with PBS and then permeabilized with 100% methanol for 10min at -20°C. Cells were washed in PBS and EdU click reaction performed following the manufacturer's instructions (Click-iT EdU AlexaFluor 647 HCS Assay, ThermoFisher, Loughborough, UK). For detection of p-ERK1/2, ERK1/2 and p-RSK, cells were blocked for 1 hour with 2% BSA/PBS at RT, followed by incubation with primary antibody diluted in 2% BSA/PBS at 4°C overnight. For background control wells 2% BSA/PBS without primary antibody was added. Cells were washed three times with PBS, and then incubated with appropriate secondary antibodies diluted 1:500 in 2% BSA/PBS containing 1μg/mL of DAPI (Sigma-Aldrich, Dorset, UK) for 1 hour at RT. Cells were washed four times with PBS and stored in 100μL PBS before imaging. Cells were imaged using an INCell Analyzer 6000 microscope (GE Healthcare, Buckinghamshire, UK) using a 10× objective lens, and typically imaging 1000–15000 individual cells (in 6 fields) per well. Image analysis to determine the mean signal intensity per cell or nuclear:cytoplasmic ratio was performed using INCell Analyzer software. To compensate for non-specific staining by p-RSK (T359) immunofluorescence in some cell lines, 1μM trametinib was utilised as a negative control as this treatment fully abolished RSK phosphorylation by immunoblot in every cell line tested (Fig. S1A-B).

Sytox & Hoechst live/dead assay

Cells were treated as described and 1 hour prior to analysis incubated with 4μM Sytox green (dead cell stain - ThermoFisher, Loughborough, UK) and 1.6μM Hoechst (live cell stain). Cells were imaged live on a InCELL 6000 high-content microscope (GE Healthcare, Buckinghamshire, UK) and the total cell number/condition and the percentage dead cells (Sytox-positive) determined by high-content image analysis using InCELL Analyzer software.

Cell cycle analysis by flow cytometry

Cells were treated as described and 1 hour prior to harvest incubated with 10μM 5-ethynyl-2-deoxyuridine (EdU; Click-iT EdU Flow Cytometry Kit, ThermoFisher, Loughborough, UK). Cells were harvested by trypsinisation and fixed with 4% paraformaldehyde/PBS for 10 min at room temperature. EdU was detected following the manufacturer's instructions, and cells were resuspended in 1μg/mL DAPI/PBS (Sigma-Aldrich, Dorset, UK). DAPI and EdU staining was assessed with a FACS LSRII (BD Biosciences, Oxford, UK), counting 10000 cells per sample. Data was analyzed using FlowJo software (FlowJo, Oregon, USA), and G1, S and G2-M cell cycle phases gated.

Annexin V-DAPI staining and flow cytometry

Cells were treated as described in the figure legends, culture medium was collected, adherent cells trypsinized and cells and media then recombined. Cells were pelleted by centrifugation (500 x g, 4°C, 5 min), resuspended in 1 mL PBS and then centrifuged again before being washed in 1 mL annexin V binding buffer (10mM HEPES/NaOH (pH 7.4), 140mM NaCl, 2.5mM CaCl2). Cells were then resuspended in 0.2 mL annexin V binding buffer containing 1μg/mL DAPI (Sigma-Aldrich, Dorset, UK) and 0.1μg/mL annexin V-FITC (BioLegend, London, UK). Annexin V/DAPI staining was assessed using an LSR II flow cytometer (BD Biosciences, Oxford, UK) and counting 10000 cells per sample. Data was analyzed using FlowJo (FlowJo, Oregon, USA) to quantify annexin V and/or DAPI positive cells.

Cell Proliferation Assay

Cell proliferation assays were carried out using Alamar Blue (ThermoFisher, Loughborough, UK) as described previously (44). Briefly, 5×10^3 cells were seeded in culture medium into 96-well plates, 24 hours before the drug treatment. Cells were incubated with compound in 0.1% (v/v) DMSO for 96 hours before viability was assessed using Alamar Blue.

Quantification of pRSK by MSD

A375 cells were seeded at 1.5×10^4 cells per well into 96-well plates and allowed to recover for 16 hours, prior to the addition of compounds for a further 4 hours. Cells were lysed by adding cell lysis buffer (Cell Signaling Technology, Massachusetts, USA) and incubating at room temperature for 20 min. MSD plates (Meso Scale Discovery, Maryland, USA) precoated with anti-pRSK antibody (Cell Signaling Technology, Massachusetts, USA) were blocked for 1 hour at room temperature, prior to incubation with equivalent amounts of protein lysate for 3 hours at room temperature. After washing, plates were incubated for 1 hour at room temperature with sulfo-tag conjugated anti-RSK detection antibodies (R&D Systems, Minneapolis, USA). Plates were washed, and read buffer added before reading on a QuickPlex SQ120 (Meso Scale Discovery, Maryland, USA).

RNA extraction and quantitative real-time PCR

Total RNA was isolated using Qiashredder and RNeasy kits (Qiagen, Manchester, UK) according to the manufacturer's instructions. 200ng of RNA was reverse-transcribed in 50µl using Taqman reverse transcription reagents (ThermoFisher, Loughborough, UK). Thermal cycle: 25°C for 5 min, 48°C for 30 min, 95°C for 5 min. The cDNA sample was diluted 1:3 in RNase-free water. 4ng of cDNA was analysed by quantitative real-time PCR using Taqman pre-validated probes (Table S1) and Universal Mastermix (ThermoFisher, Loughborough, UK). A Bio-Rad CFX96 system was used with the following cycling conditions: 50°C for 2 min, 95°C for 10 min, 95°C for 3s and 60°C for 30s, with the final 2 steps repeated 40 times. Fluorescence output was considered directly proportional to the input cDNA concentration and was normalised against β-actin or 18S expression.

Microarray gene expression profiling

For microarray data analysis, RNA samples were profiled from A375, COLO205 and HCT116 cells treated with SCH772984, GDC-0994 or DMSO for 24hrs (3 independent biological replicates per treatment and 4 DMSO replicates). The whole genome expression profiling was carried out using Illumina HumanHT-12v4 expression beadchip platform. The raw un-normalised data was exported from GenomeStudio and analysed using the *limma* R package (45). The probe intensities were background corrected using negative control probes and quantile normalised using negative and positive control probes using the limma *neqc* function. After normalisation, probes were then filtered according to their annotation quality and selected only those with an inter quartile range (IQR) > 0.5. The function *lmFit* was used to fit linear models on expression values of genes. The function *eBayes* was used to calculate differential expression between untreated and treated samples using moderated t-statistics. Pvalues were corrected for multiple testing using the Benjamini and Hochberg method (46). Following this correction, genes with more than 2-fold expression change and adjusted Pvalues <0.01 were considered significant. Enrichment analysis of gene ontologies of differentially expressed genes was performed using the clusterProfiler R package (47). Microarray data are available in the ArrayExpress database (http://www.ebi.ac.uk/arrayexpress) under accession number E-MTAB-7959.

ERK2 Kinase Assay

ERK2 kinase activity was determined using a time-resolved fluorescence (TRF) activity assay. ERK2 (0.25nM) was incubated with the substrates ATF2-GFP (0.4µM) and ATP (20µM) in 50mM Tris pH 7.5, 10mM $MgCl_2$, 1mM EGTA, 0.01% Triton X100, 1mM DTT, and 2.5% dimethyl sulfoxide (DMSO), with shaking at room temperature for 30 min. Reactions were stopped by the addition of stop and detection mix, containing 25mM EDTA and 2nM Tb-pATF2 antibody in TR-FRET dilution buffer (Life Technologies, Paisley, UK), and the plate was incubated with shaking at room temperature for 1 hour. Upon excitation at 340nm, fluorescence was measured at 520nm and 495nm using a Pherastar plate reader (BMG Labtech, Germany).

Protein Expression, Purification, and Crystallography

Full length human ERK2 (hERK2) was cloned into pET30a with a noncleavable MAHHHHHH N-terminal tag. hERK2 was expressed in *E. coli* BL21(DE3) and nonphosphorylated hERK2 (confirmed by LCMS) was purified using sequential Ni-HiTRAP, desalt, Resource-Q, and S75 26/60 column steps. hERK2 was crystallized under conditions adapted from Aronov et al., (2009) (30) and crystals were soaked in a solution equivalent to the crystallization solution but also containing 0.1–100mM ligand, 10mM DTT, and 10% DMSO. Crystals were cryo-protected using crystallization solution containing 35% 2KMPEG final. X-ray diffraction data were collected using both in-house and synchrotron X-ray sources. X-ray crystal structures are available in the wwPDB (www.wwpdb.org) under the indicated PBD ID codes.

Results

ERKi display distinct binding modes which influence their ability to modulate ERK1/2 phosphorylation

We studied two dmERKi, Compound 27 and SCH772984 (21,25), two catERKi, GDC-0994 and BVD-523 (16,18), and LY-3214996, (19) (Fig. 1A). Crystal structures of these ERKi bound to ERK2 revealed distinct binding modes between the dmERKi and catERKi (Fig. 1B). GDC-0994 and BVD-523 behaved as typical ATP-competitive inhibitors, binding to the active form of ERK2 and occupying the ATP binding pocket (pdb: 4nif). GDC-0994 exploited a 2-amino-pyrimidine scaffold to bind to the ERK2 pocket. Its donor-acceptor motif formed a double H-Bond pattern with the “hinge” region residue, Met108. The molecule ended with a terminal 4-chloro-3-fluorophenyl ring sitting under the P-Loop. The Tyr36 phenol ring here was in an "out" conformation and formed a pi−pi stacking interaction with Tyr64 on the C-α helix (18,25). BVD-523 exhibited a very similar binding mode, with the Tyr36 phenol ring in an "out" conformation. LY-3214996 bound to ERK2 in a similar manner to BVD-523 and GDC-0994, prompting us to predict that it would act as a catERKi. In contrast, whilst Compound 27 and SCH772984 also occupied the ERK2 ATP binding site, they imposed a conformational change upon the Tyr36 side chain such that it folded beneath the P-loop (Tyr36 “in”), in the pocket occupied by the terminal rings of GDC-0994 and BVD-523. Thus, catERKi and dmERKi have distinct binding modes, consistent with a report that occupancy of the second pocket, displacing Tyr36, correlated with modulation of p-ERK1/2 levels (25).

We monitored the effects of these ERKi on ERK1/2 T-E-Y phosphorylation (p-ERK1/2) and ERK1/2 catalytic activity (phosphorylation of RSK, an ERK1/2 substrate) following 2h treatment. In $KRAS^{mut}$ HCT116 (Fig. 1C, S2B) and Capan-1 (Fig. 1C, S3B) cells the catERKi BVD-523 and GDC-0994 increased p-ERK1/2 levels, reflecting loss of ERK1/2-mediated negative feedback. LY-3214996 treatment also promoted p-ERK1/2 accumulation, validating our prediction that it acts as a catERKi. In contrast, the dmERKi SCH772984 and Compound 27 induced a dose-dependent inhibition of ERK1/2

phosphorylation, comparable to the MEKi (Fig. 1C, S2B, S3B). In contrast to $KRAS^{mut}$ cells, $BRAF^{V600E}$ mutant cells lines display little ERK1/2 rebound following ERK1/2 pathway inhibition, as $BRAF^{V600E}$ activity is insensitive to ERK1/2-mediated negative feedback (34,48). Consequently in $BRAF^{V600E}$ COLO205 (Fig. 1C, S2A) and A375 (Fig. 1C, S3A) cells catERKi did not drive accumulation of p-ERK1/2, instead inhibiting ERK1/2 phosphorylation to varying degrees, although not to the extent of dmERKi. Thus, ERKi exhibit a spectrum of abilities to antagonise ERK1/2 phosphorylation. The mechanistic differences between dmERKi and catERKi were retained *in vivo*, where Compound 27, but not GDC-0994, inhibited ERK1/2 phosphorylation in COLO205 xenografts (Fig. 1D).

Utilising p-RSK as a biomarker of ERK1/2 activity revealed that dmERKi exhibited enhanced potency compared to catERKi across both KRAS and $BRAF^{V600E}$ mutant cell lines (Fig. 1C, S2, S3). This increased potency could be a property of the binding mode of dmERKi, or could reflect their ability to block the active conformation of ERK1/2, in addition to inhibiting catalysis.

Dual-mechanism ERKi are more potent than catalytic ERKi, but both prevent ERK1/2 pathway rebound as effectively as 'feedback buster' MEKi

We next assessed the effects of ERKi on p-ERK1/2 levels and pathway rebound. To differentiate MoA from compound potency, compound concentrations were normalised for potency, by selecting the lowest concentration that inhibited >90% of RSK phosphorylation (Table S2, Fig. 1C, S2, S3). In HCT116 (Fig. 2A-B, S4A) and Capan-1 (Fig. S4B-C) cells catERKi promoted p-ERK1/2 accumulation over time, including a 5-6 fold increase with BVD-523 and LY-3214996. In contrast, dmERKi caused a rapid, strong inhibition of ERK1/2 phosphorylation, which then recovered from 4-8 hours onwards. Despite this restoration of p-ERK1/2, p-RSK levels were still robustly suppressed by dmERKi (Fig. 2B, S4C). Thus, dmERKi were more effective at inhibiting ERK1/2 catalytic activity than ERK1/2 phosphorylation.

Feedback relief after ERK1/2 inhibition enables pathway rebound over time. Indeed, the 'feedback buster' MEKi trametinib delayed and reduced pathway rebound (p-RSK levels) compared to selumetinib, which does not block MEK1/2 phosphorylation by RAF (Fig. 2B, S4C) (32–34). Interestingly, both dmERKi and catERKi prevented rebound in a comparable manner to trametinib, however there were no distinct trends by MoA (Fig. 2B, S4C). BVD-523 was the only ERKi that totally prevented pathway rebound at the normalised concentration utilised (Fig. 2B, S4C).

We also examined all compounds across multiple concentrations using dose/time matrices for each compound in HCT116 and Capan-1 cells (Fig. 2C-D, S5). DmERKi displayed superior potency relative to catERKi across all treatment times in both cell lines (Fig. 2C, S5A). Compound 27, SCH772984, GDC-0994, LY-3214996 and trametinib displayed similar pathway rebound following the initial loss of p-RSK, whereas selumetinib or PD184352 displayed more dramatic pathway rebound. BVD-523 was unique in fully abolishing pathway rebound (Fig. 2C, S5A). Consistent with previous data, catERKi induced a strong accumulation of p-ERK1/2, whilst dmERKi caused an initial reduction in p-ERK1/2 followed by gradual recovery over time (Fig. 2D, S5B). Together these data demonstrate that when utilised at comparable concentrations all ERKi prevent ERK1/2 pathway rebound as effectively as trametinib; however, dmERKi display increased potency relative to catERKi (Fig. 1C, 2C), most likely reflecting their novel binding mode. Interestingly, BVD-523-induced p-ERK1/2 accumulation peaked between 2-8h before declining (Fig. 2D, S5B); this decline correlated with a progressive loss of total ERK1/2 (>75% reduction) (Fig. S5C-D), which could explain the apparent durability of BVD-523 mediated ERK1/2 pathway inhibition. The cause of this loss of total ERK1/2 is currently under investigation.

Catalytic, but not dual mechanism, ERKi induce the nuclear accumulation of p-ERK1/2

T-E-Y phosphorylation induces ERK1/2 nuclear translocation (4), therefore catERKi which induce the accumulation of p-ERK1/2 (Fig. 1C, 2B-D) should promote the nuclear accumulation of inhibited p-ERK1/2; we tested this by immunofluorescence and high-content microscopy. In HCT116 cells all catERKi promoted a striking nuclear accumulation of p-ERK1/2, and more subtle nuclear redistribution of total ERK1/2 (Fig. 3A-B). In contrast, whilst dmERKi or MEKi abolished p-ERK1/2 levels, only MEKi treatment induced a strong cytoplasmic redistribution of total ERK1/2 (Fig. 3A-B), suggesting that preventing both MEK1/2 activity and ERK1/2 phosphorylation is essential to prevent the release of ERK1/2 from MEK1/2 and retain ERK1/2 in the cytoplasm. Consistent results were observed in COLO205, A375 and Capan-1 cells, with changes in p-ERK1/2 localisation varying in proportion with the level of p-ERK1/2 accumulation (Fig. S6A-B). To confirm that the nuclear p-ERK1/2 that accumulated following catERKi treatment was inhibited, we quantified levels of the ERK1/2-dependent transcripts DUSP6 and Sprouty-2; both were suppressed to comparable levels by dmERKi, catERKi or MEKi demonstrating that catERKi-driven nuclear accumulation of p-ERK1/2 was not able to promote ERK1/2-dependent gene expression (Fig. 3C).

If the nuclear accumulation of ERK1/2 following catERKi treatment is sustained in the absence of drug, this could alter the kinetics of pathway reactivation, potentially accelerating ERK1/2-dependent gene expression. To address this, HCT116 cells were treated with ERKi for 24h, and then switched to drug-free media for a 4-hour time-course. Following wash-off of GDC-0994 or LY-3214996, p-ERK1/2 accumulation and nuclear localisation rapidly decreased to basal levels within 2 hours (Fig. 3D-E). This correlated with a rapid reactivation of ERK1/2, inducing peak p-RSK 1 hour following drug withdrawal (Fig. 3F-G, S7A). In contrast, p-ERK1/2 nuclear accumulation was retained following BVD-523 wash-off (Fig. 3E); however, this correlated with a very slow recovery in p-RSK levels (Fig. 3G, S7-C). Withdrawal of dmERKi or MEKi had varying effects on pathway reactivation, with selumetinib displaying a rapid increase in p-RSK levels, comparable with GDC-0994 and LY-3214996, whereas the withdrawal of Compound 27, SCH772984 or trametinib elicited a more delayed response (Fig. 3F-G, S7C). Wash-off of selumetinib induced a more rapid re-expression of DUSP5 than GDC-0994 or LY-3214996 (Fig. 3F-G, S7A). This, coupled with the rapid loss of nuclear p-ERK1/2 upon GDC-0994 or LY-3214996 withdrawal, indicates the catERKi are unlikely to facilitate accelerated ERK1/2-dependent gene expression upon drug withdrawal, due to feedback controls rapidly restoring homeostatic ERK1/2 phosphorylation and cellular localisation. With the exception of BVD-523, the kinetics of pathway reactivation following compound withdrawal correlated with compound potency, not compound target or MoA. This could be due to more potent compounds having a slower off-rate, thereby remaining bound to ERK1/2 or MEK1/2 for longer following the withdrawal of drug-containing media (49).

The dual-mechanism ERKi SCH772984 induces a more robust inhibition of ERK1/2-dependent target genes than catalytic ERKi GDC-0994

We next investigated whether, by preventing ERK1/2 from entering the nucleus (Fig. 3A-B, S6), dmERKi exerted a more robust effect on ERK1/2-dependent gene expression. We treated HCT116, COLO205 and A375 cells with concentrations of SCH772984 or GDC-0994 that induced a comparable growth arrest (Table S3) and performed gene expression profiling using microarrays. SCH772984 induced a more comprehensive inhibition of 10 well-established ERK1/2 target genes across all cell lines (Fig. 4A). We also compared global gene expression changes (Fig. S8A); whilst both compounds altered the expression of a common set of genes, SCH772984 selectively altered the expression of a significant number of further genes (Fig. 4B). Gene ontology (GO) analysis of common or SCH772984-specific downregulated gene signatures revealed that many of the most significantly

downregulated processes were involved in DNA-replication or cell cycle progression (Fig. 4C). Many GO terms identified for SCH772984-specific downregulated genes were the same as those identified for the common downregulated genes, indicating that SCH772984 was inhibiting the same processes as GDC-0994 but in a more comprehensive manner (Fig. 4C).

ERK2 is proposed to act as a kinase-independent transcriptional repressor of interferon signalling by directly binding DNA (39). The 'response to type I interferon' GO term was far more significantly upregulated in SCH772984-treated HCT116 cells (p value $1.08x10^{-8}$) compared to either GDC-0994 or DMSO (Fig. 4D); within this signature were multiple genes that ERK2 has been shown to bind directly to and repress in a kinase-independent manner (Fig. 4E) (39). Treatment of HCT116 cells with dmERKi or MEKi consistently caused a greater upregulation of these ERK2-repressed genes relative to catERKi, at concentrations that induced comparable downregulation of the established ERK1/2 target genes DUSP6 and SPRY2 (Fig. 4F). Furthermore, the upregulation of these genes did not correlate with the ability of ERKi to repress ERK1/2 target genes (Fig. S8B), indicating that this property of dmERKi was likely due to their MoA, and ability to retain ERK1/2 in the cytoplasm, not their enhanced potency relative to catERKi. The ability of some ERKi, notably BVD-523, to reduce total ERK1/2 (Fig. 2B) could also help to facilitate the de-repression of these ERK2 bound genes. Together these data indicate that SCH772984, a dmERKi, differentially regulates a larger pool of genes and processes than GDC-0994, a catERKi, even when doses are normalised for pathway inhibition. This likely reflects the ability of SCH772984 to prevent MEK1/2-catalysed phosphorylation-dependent conformational changes and nuclear-localisation, compared to simple inhibition of catalytic activity of ERK1/2 by GDC-0994. However, the preferential upregulation of interferon-induced genes by SCH772984 and Compound 27 suggests that only dmERKi have the potential to inhibit proposed nuclear kinase-independent functions of ERK1/2 (35,36,38,39).

The anti-proliferative effects of ERKi correlate with their ability to inhibit ERK1/2 catalytic activity

To determine whether the increased potency (loss of p-RSK) of dmERKi relative to catERKi (Fig. 1C, 2C, S5A) translated into increased biological efficacy we assessed proliferation of a panel of eight colorectal cancer (CRC) cell lines (Fig. 5A-B, S9-10) using high-content imaging to detect EdU incorporation and p-RSK or p-ERK1/2 in the same cell population following a 24h compound treatment. DmERKi demonstrated superior anti-proliferative potency across all cell lines tested, irrespective of BRAF or KRAS mutant status (Fig. 5B). All ERKi displayed reduced efficacy in $KRAS^{mut}$ cell lines relative to $BRAF^{mut}$ (Fig. 5C), reflecting innate resistance by additional KRAS effector signalling pathways. Relating p-RSK and EdU incorporation revealed that the anti-proliferative effects of both catERKi and dmERKi correlated with their ability to inhibit ERK1/2 catalytic activity (Fig. 5D). In contrast, ERK1/2 phosphorylation or subcellular localisation did not correlate with compound efficacy (Fig. 5A, S9-10). Consistent with the effects of feedback relief and pathway rebound, in almost all cases the 72h dose-response curves were right-shifted relative to the 24h, indicating that a greater compound concentration was required to achieve comparable inhibition (Fig. S11A, 5A, S9-10). Regardless, the anti-proliferative effects of all ERKi or MEKi correlated with their ability to inhibit ERK1/2 catalytic activity, and there were no major differences between dmERKi and catERKi (Fig. S11B). Thus, proposed kinase-independent functions of ERK1/2 appeared not to play crucial roles in regulating proliferation in response to ERKi treatment, though they could mediate other cellular phenotypes.

MEK1/2 inhibition promotes a cytostatic response in most ERK1/2 pathway mutant cell lines, due to the loss of ERK1/2-dependent transcription of D-type cyclins promoting a G1 cell cycle arrest (9,13). To investigate whether ERKi induce a comparable response we treated eight CRC cell lines with ERKi or MEKi for 72h and determined the total cell number (Fig. S12A) and the proportion of dead cells

(Fig. S12B). Both dmERKi and catERKi induced a predominantly cytostatic response in the majority of cell lines (Fig. S12A-B). Where cell death did occur it was induced to a similar magnitude by all ERKi (Fig. S12B), and Annexin V staining revealed this to be apoptotic cell death (Fig. S12C). To further characterise the mechanism of ERKi-induced proliferative arrest we examined the cell cycle profiles of COLO205 and HCT116 cells following ERKi treatment. Whilst dmERKi promoted a G1 arrest in both cell lines, the catERKi BVD-523 and LY-3214996 promoted a G2/M arrest in HCT116 cells, but not COLO205 (Fig. S13A). This G2/M arrest correlated with the strong nuclear accumulation of p-ERK1/2 seen in catERKi treated HCT116, but not COLO205 cells (Fig. S13B). ERK1/2 have been suggested to drive G1 progression through a kinase-independent manner, via ERK1/2 displacing Rb from lamin A, to facilitate CDK-dependent Rb phosphorylation (38). Therefore, we hypothesised that nuclear p-ERK1/2 induced by catERKi might act in a kinase-independent manner to promote G1 progression, thus enabling a G2/M checkpoint arrest due to the inhibition of ERK1/2 catalytic activity. Indeed, BVD-523 and LY-3214996 treated HCT116 cells retained Rb phosphorylation even though CyclinD1 was decreased to levels comparable with that induced by dmERKi or MEKi, whereas Rb phosphorylation was lost following treatment with all ERKi in COLO205 cells (Fig. S13C). BVD-523 and LY-3214996 treated HCT116 cells also retained expression of the G2 markers Cyclin A and Cyclin B (Fig. S13C), but were p-Histone H3 negative (Fig. S13D) consistent with arrest at the G2/M checkpoint. However, this phenotype was not consistent across a range of other cell lines (Fig. S14A-C), despite the strong induction of nuclear p-ERK1/2 in some cell lines (Fig. S14B).

To model the ability of cells to acquire resistance to ERKi we treated HCT116 and COLO205 cells with doses of ERKi normalised to induce comparable pathway inhibition and short-term growth arrest, then monitored their growth (Fig. 6A, S15A) and ability to proliferate in drug (Fig. 6B, S15B) over time. In HCT116 cells, resistance emerged slightly more slowly with the five ERKi compared to the MEKi (PD184352) but there was no clear trend in terms of ERKi MoA (Fig. 6A). In all cases HCT116 or COLO205 cells adapted to ERKi treatment by reinstating ERK1/2 signalling and this was associated with an increase in KRAS expression in HCT116 (Fig. 6C-D), or BRAF expression in COLO205 (Fig. S15C-D). This is consistent with our previous demonstration that HCT116 and COLO205 cells adapt to MEKi by amplifying their driving oncogene (13). Consistent with these mechanistic similarities, all ERKi or MEKi resistant cell lines displayed cross-resistance to other ERKi or MEKi (Fig. S16A-B). However, surprisingly ERKi-resistant HCT116 cells displayed a greater degree of cross-resistance to other ERKi than they did to the MEKi PD184352 (Fig. S16A).

Discussion

In addition to inhibiting catalysis, ERKi entering the clinic possess a range of abilities to modulate the phosphorylation of ERK1/2 by MEK1/2 (16,20,21,25,28). The biological consequences of these different MoA are largely unknown and prompted this study. DmERKi possess a unique binding mode that mediates a conformational change in the Tyr36 side chain of the EKR1/2 P-loop (Fig. 1B)(25,49); such inhibitors robustly suppress ERK1/2 T-E-Y phosphorylation in both BRAF and RAS mutant cell lines (Fig. 1C). Furthermore, dmERKi consistently exhibited enhanced potency (Fig. 1C) and more durable ERK1/2 pathway suppression (Fig. 2C, S5A). However, in contrast to MEKi (32–34), the ability of dmERKi to inhibit ERK1/2 phosphorylation did not appear to delay or reduce pathway rebound relative to catERKi when used at comparable concentrations (Fig. 2). Instead, both catERKi and dmERKi displayed similar rebound profiles to the 'feedback buster' MEKi trametinib (Fig. 2). This ability to induce durable pathway inhibition could be a characteristic of targeting the terminal kinase in the ERK1/2 pathway, and is consistent with reports that greater levels of BRAF amplification are required to generate resistance to ERKi than to MEKi or BRAFi (50).

By blocking T-E-Y phosphorylation, dmERKi did not elicit the striking nuclear accumulation of p-ERK1/2 that was observed following catERKi treatment (Fig. 3A-B, S6). Changes in p-ERK1/2 localisation were coupled with more subtle changes in the localisation of total ERK1/2 (Fig. 3A-B, S7), reflecting the small fraction of ERK1/2 known to be phosphorylated at any one time (42) and the large proportion bound in scaffold complexes. This ability of dmERKi to inhibit nuclear localisation of ERK1/2 could explain their ability to facilitate more robust suppression of ERK1/2-dependent gene expression than catERKi (Fig. 4) and therefore contribute to the increased anti-proliferative efficacy observed with dmERKi (Fig. 5A-B). In contrast, the nuclear accumulation of p-ERK1/2 driven by catERKi would increase the likelihood that any ERK1/2 activity that escapes inhibition would be able to target transcription factors and restore pro-survival and proliferative transcription programs. In addition, catERKi-driven nuclear p-ERK1/2 has the potential to sustain nuclear non-catalytic functions of ERK1/2, such as its role as a transcriptional repressor of interferon responsive genes (39), that appear to be suppressed by dmERKi treatment (Fig. 4E-F). The nuclear accumulation of p-ERK1/2 was rapidly lost following catERKi withdrawal, indicating that the nuclear p-ERK1/2 was inhibitor bound and that this localisation does not influence the kinetics of pathway reactivation as compound activity is lost (Fig. 3D-G, S7).

Whilst both dmERKi were consistently more potent we found that the anti-proliferative effects of all ERKi ultimately correlated with their ability to inhibit ERK1/2 catalytic activity rather than their distinct MoA (Fig. 5A, 5D S9-11). At concentrations of each ERKi that inhibited the same proportion of p-RSK (a measure of ERK1/2 inhibition) all compounds displayed a similar ability to inhibit proliferation, despite clear differences in p-ERK1/2 levels and localisation. Therefore, the differences in regulation of ERK1/2 phosphorylation and localisation associated with each ERKi MoA did not influence their anti-proliferative activity, though we cannot rule out effects on other cellular phenotypes such as cell motility or survival.

In summary, the dmERKi tested exhibited a distinct binding mode, increased potency and more durable pathway inhibition. dmERKi also prevented ERK1/2 nuclear localisation, thereby phenocopying strong 'feedback buster' MEKi such as trametinib. As a consequence, dmERKi exhibited enhanced suppression of ERK1/2-dependent gene expression, both for selected ERK1/2 target genes and in global transcriptomic analysis. Nuclear accumulation of p-ERK1/2 driven by catERKi has the potential to sustain non-catalytic functions of ERK1/2 (the majority of which occur in the nucleus and therefore could be regulated by nuclear translocation). Whilst this seems less important for anti-proliferative efficacy it may contribute to other cancer hallmarks. Together these results suggest that a dual-mechanism profile is likely to be advantageous for ERKi development.

Author Contributions

Conception and design: A.M.K, J.M.M and S.J.C.

Development of methodology: A.M.K, K.B, A.C and B.G.

Acquisition of data (provided animals, acquired and managed patients, provided facilities, etc.): A.M.K, K.B, E.M, A.C, B.G, M.O and R.O.

Analysis and interpretation of data (e.g., statistical analysis, biostatistics, computational analysis): A.M.K and H.K.S.

Writing, review, and/or revision of the manuscript: A.M.K, J.M.M and S.J.C.

Administrative, technical, or material support (i.e., reporting or organizing data, constructing databases): A.M.K and H.K.S.

Study supervision: S.J.C and J.M.M.

Acknowledgements

We would like to thank past and present members of the Cook laboratory and Babraham Institute Science Services for their support throughout this study, especially Simon Walker, Hanneke Okkenhaug (Imaging) and Matthew Sale. This study was funded by a grant from Astex Pharmaceuticals awarded through the Milner Therapeutics Consortium (A.M.K. and S.J.C.) and Institute Strategic Programme Grants BB/J004456/1 and BB/P013384/1 from BBSRC (S.J.C., K.B. & R.O.).

References

1. Cargnello M, Roux PP. Activation and Function of the MAPKs and Their Substrates, the MAPK-Activated Protein Kinases. Microbiol Mol Biol Rev. 2011;75:50–83.

2. Lavoie H, Therrien M. Regulation of RAF protein kinases in ERK signalling. Nature Reviews Molecular Cell Biology. 2015;16:281–98.

3. Karnoub AE, Weinberg RA. Ras oncogenes: split personalities. Nature Reviews Molecular Cell Biology. 2008;9:517.

4. Plotnikov A, Zehorai E, Procaccia S, Seger R. The MAPK cascades: Signaling components, nuclear roles and mechanisms of nuclear translocation. Biochimica et Biophysica Acta (BBA) - Molecular Cell Research. 2011;1813:1619–33.

5. Dougherty MK, Müller J, Ritt DA, Zhou M, Zhou XZ, Copeland TD, et al. Regulation of Raf-1 by Direct Feedback Phosphorylation. Molecular Cell. 2005;17:215–24.

6. Kidger AM, Keyse SM. The regulation of oncogenic Ras/ERK signalling by dual-specificity mitogen activated protein kinase phosphatases (MKPs). Seminars in Cell & Developmental Biology. 2016;50:125–32.

7. Masoumi-Moghaddam S, Amini A, Morris DL. The developing story of Sprouty and cancer. Cancer Metastasis Rev. 2014;33:695–720.

8. Montagut C, Settleman J. Targeting the RAF–MEK–ERK pathway in cancer therapy. Cancer Letters. 2009;283:125–34.

9. Caunt CJ, Sale MJ, Smith PD, Cook SJ. MEK1 and MEK2 inhibitors and cancer therapy: the long and winding road. Nat Rev Cancer. 2015;15:577–92.

10. Holderfield M, Deuker MM, McCormick F, McMahon M. Targeting RAF kinases for cancer therapy: BRAF-mutated melanoma and beyond. Nature Reviews Cancer. 2014;14:455.

11. Kidger AM, Sipthorp J, Cook SJ. ERK1/2 inhibitors: New weapons to inhibit the RAS-regulated RAF-MEK1/2-ERK1/2 pathway. Pharmacology & Therapeutics [Internet]. 2018 [cited 2018 Apr 17]; Available from: http://www.sciencedirect.com/science/article/pii/S0163725818300329

12. Ahronian LG, Sennott EM, Allen EMV, Wagle N, Kwak EL, Faris JE, et al. Clinical Acquired Resistance to RAF Inhibitor Combinations in BRAF-Mutant Colorectal Cancer through MAPK Pathway Alterations. Cancer Discov. 2015;5:358–67.

13. Little AS, Balmanno K, Sale MJ, Newman S, Dry JR, Hampson M, et al. Amplification of the Driving Oncogene, KRAS or BRAF, Underpins Acquired Resistance to MEK1/2 Inhibitors in Colorectal Cancer Cells. Sci Signal. 2011;4:ra17–ra17.

14. Corcoran RB, Dias-Santagata D, Bergethon K, Iafrate AJ, Settleman J, Engelman JA. BRAF Gene Amplification Can Promote Acquired Resistance to MEK Inhibitors in Cancer Cells Harboring the BRAF V600E Mutation. Sci Signal. 2010;3:ra84–ra84.

15. Poulikakos PI, Persaud Y, Janakiraman M, Kong X, Ng C, Moriceau G, et al. RAF inhibitor resistance is mediated by dimerization of aberrantly spliced BRAF(V600E). Nature. 2011;480:387–90.

16. Germann UA, Furey BF, Markland W, Hoover RR, Aronov AM, Roix JJ, et al. Targeting the MAPK Signaling Pathway in Cancer: Promising Preclinical Activity with the Novel Selective ERK1/2 Inhibitor BVD-523 (Ulixertinib). Mol Cancer Ther. 2017;16:2351–63.

17. Li BT, Janku F, Patel MR, Sullivan RJ, Flaherty K, Buchbinder EI, et al. First-in-class oral ERK1/2 inhibitor Ulixertinib (BVD-523) in patients with advanced solid tumors: Final results of a phase I dose escalation and expansion study. JCO. 2017;35:2508–2508.

18. Blake JF, Burkard M, Chan J, Chen H, Chou K-J, Diaz D, et al. Discovery of (S)-1-(1-(4-Chloro-3-fluorophenyl)-2-hydroxyethyl)-4-(2-((1-methyl-1H-pyrazol-5-yl)amino)pyrimidin-4-yl)pyridin-2(1H)-one (GDC-0994), an Extracellular Signal-Regulated Kinase 1/2 (ERK1/2) Inhibitor in Early Clinical Development. J Med Chem. 2016;59:5650–60.

19. A Study of LY3214996 Administered Alone or in Combination With Other Agents in Participants With Advanced/Metastatic Cancer - Full Text View - ClinicalTrials.gov [Internet]. 2016 [cited 2017 Aug 31]. Available from: https://clinicaltrials.gov/ct2/show/NCT02857270

20. Moschos SJ, Sullivan RJ, Hwu W-J, Ramanathan RK, Adjei AA, Fong PC, et al. Development of MK-8353, an orally administered ERK1/2 inhibitor, in patients with advanced solid tumors. JCI Insight [Internet]. 2018 [cited 2018 Jul 17];3. Available from: https://insight.jci.org/articles/view/92352

21. Morris EJ, Jha S, Restaino CR, Dayananth P, Zhu H, Cooper A, et al. Discovery of a Novel ERK Inhibitor with Activity in Models of Acquired Resistance to BRAF and MEK Inhibitors. Cancer Discov. 2013;3:742–50.

22. Study of ASTX029 in Subjects With Advanced Solid Tumors - Full Text View - ClinicalTrials.gov [Internet]. 2018 [cited 2019 Jan 21]. Available from: https://clinicaltrials.gov/ct2/show/NCT03520075

23. A Phase I Clinical Study With Investigational Compound LTT462 in Adult Patients With Specific Advanced Cancers - Full Text View - ClinicalTrials.gov [Internet]. 2016 [cited 2017 Aug 31]. Available from: https://clinicaltrials.gov/ct2/show/NCT02711345

24. First-in-Human Study of KO-947 in Non-Hematological Malignancies - Full Text View - ClinicalTrials.gov [Internet]. 2017 [cited 2017 Aug 31]. Available from: https://clinicaltrials.gov/ct2/show/NCT03051035

25. Heightman TD, Berdini V, Braithwaite H, Buck IM, Cassidy M, Castro J, et al. Fragment-Based Discovery of a Potent, Orally Bioavailable Inhibitor That Modulates the Phosphorylation and Catalytic Activity of ERK1/2. J Med Chem. 2018;61:4978–92.

26. Lechtenberg BC, Mace PD, Sessions EH, Williamson R, Stalder R, Wallez Y, et al. Structure-Guided Strategy for the Development of Potent Bivalent ERK Inhibitors. ACS Med Chem Lett. 2017;8:726–31.

27. Ward RA, Colclough N, Challinor M, Debreczeni JE, Eckersley K, Fairley G, et al. Structure-Guided Design of Highly Selective and Potent Covalent Inhibitors of ERK1/2. J Med Chem. 2015;58:4790–801.

28. Ward RA, Bethel P, Cook C, Davies E, Debreczeni JE, Fairley G, et al. Structure-Guided Discovery of Potent and Selective Inhibitors of ERK1/2 from a Modestly Active and Promiscuous Chemical Start Point. J Med Chem [Internet]. 2017 [cited 2017 Apr 21]; Available from: http://dx.doi.org/10.1021/acs.jmedchem.7b00267

29. Lim J, Kelley EH, Methot JL, Zhou H, Petrocchi A, Chen H, et al. Discovery of 1-(1H-Pyrazolo[4,3-c]pyridin-6-yl)urea Inhibitors of Extracellular Signal-Regulated Kinase (ERK) for the Treatment of Cancers. J Med Chem. 2016;59:6501–11.

30. Aronov AM, Tang Q, Martinez-Botella G, Bemis GW, Cao J, Chen G, et al. Structure-Guided Design of Potent and Selective Pyrimidylpyrrole Inhibitors of Extracellular Signal-Regulated Kinase (ERK) Using Conformational Control. J Med Chem. 2009;52:6362–8.

31. Bagdanoff JT, Jain R, Han W, Zhu S, Madiera A-M, Lee PS, et al. Tetrahydropyrrolo-diazepenones as inhibitors of ERK2 kinase. Bioorganic & Medicinal Chemistry Letters. 2015;25:3788–92.

32. Hatzivassiliou G, Haling JR, Chen H, Song K, Price S, Heald R, et al. Mechanism of MEK inhibition determines efficacy in mutant KRAS- versus BRAF-driven cancers. Nature. 2013;501:232–6.

33. Ishii N, Harada N, Joseph EW, Ohara K, Miura T, Sakamoto H, et al. Enhanced Inhibition of ERK Signaling by a Novel Allosteric MEK Inhibitor, CH5126766, That Suppresses Feedback Reactivation of RAF Activity. Cancer Res. 2013;73:4050–60.

34. Lito P, Saborowski A, Yue J, Solomon M, Joseph E, Gadal S, et al. Disruption of CRAF-Mediated MEK Activation Is Required for Effective MEK Inhibition in KRAS Mutant Tumors. Cancer Cell. 2014;25:697–710.

35. Shapiro PS, Whalen AM, Tolwinski NS, Wilsbacher J, Froelich-Ammon SJ, Garcia M, et al. Extracellular Signal-Regulated Kinase Activates Topoisomerase IIα through a Mechanism Independent of Phosphorylation. Mol Cell Biol. 1999;19:3551–60.

36. Cohen-Armon M, Visochek L, Rozensal D, Kalal A, Geistrikh I, Klein R, et al. DNA-Independent PARP-1 Activation by Phosphorylated ERK2 Increases Elk1 Activity: A Link to Histone Acetylation. Molecular Cell. 2007;25:297–308.

37. Camps M, Nichols A, Gillieron C, Antonsson B, Muda M, Chabert C, et al. Catalytic Activation of the Phosphatase MKP-3 by ERK2 Mitogen-Activated Protein Kinase. Science. 1998;280:1262–5.

38. Rodríguez J, Calvo F, González JM, Casar B, Andrés V, Crespo P. ERK1/2 MAP kinases promote cell cycle entry by rapid, kinase-independent disruption of retinoblastoma–lamin A complexes. The Journal of Cell Biology. 2010;191:967–79.

39. Hu S, Xie Z, Onishi A, Yu X, Jiang L, Lin J, et al. Profiling the Human Protein-DNA Interactome Reveals ERK2 as a Transcriptional Repressor of Interferon Signaling. Cell. 2009;139:610–22.

40. Workman P, Aboagye EO, Balkwill F, Balmain A, Bruder G, Chaplin DJ, et al. Guidelines for the welfare and use of animals in cancer research. Br J Cancer. 2010;102:1555–77.

41. Hollands C. THE ANIMALS (SCIENTIFIC PROCEDURES) ACT 1986. The Lancet. 1986;328:32–3.

42. Sale MJ, Balmanno K, Saxena J, Ozono E, Wojdyla K, McIntyre RE, et al. MEK1/2 inhibitor withdrawal reverses acquired resistance driven by BRAF V600E amplification whereas KRAS G13D amplification promotes EMT-chemoresistance. Nature Communications. 2019;10:2030.

43. Caunt ChristopherJ, Kidger AndrewM, Keyse StephenM. Visualizing and Quantitating the Spatiotemporal Regulation of Ras/ERK Signaling by Dual-Specificity Mitogen-Activated Protein Phosphatases (MKPs). In: Pulido R, editor. Protein Tyrosine Phosphatases [Internet]. Springer New York; 2016 [cited 2016 Sep 9]. page 197–215. Available from: http://dx.doi.org/10.1007/978-1-4939-3746-2_12

44. Squires MS, Feltell RE, Wallis NG, Lewis EJ, Smith D-M, Cross DM, et al. Biological characterization of AT7519, a small-molecule inhibitor of cyclin-dependent kinases, in human tumor cell lines. Mol Cancer Ther. 2009;8:324–32.

45. Ritchie ME, Phipson B, Wu D, Hu Y, Law CW, Shi W, et al. limma powers differential expression analyses for RNA-sequencing and microarray studies. Nucleic Acids Res. 2015;43:e47–e47.

46. Benjamini Y, Hochberg Y. Controlling the False Discovery Rate: A Practical and Powerful Approach to Multiple Testing. Journal of the Royal Statistical Society Series B (Methodological). 1995;57:289–300.

47. Yu G, Wang L-G, Han Y, He Q-Y. clusterProfiler: an R Package for Comparing Biological Themes Among Gene Clusters. OMICS: A Journal of Integrative Biology. 2012;16:284–7.

48. Friday BB, Yu C, Dy GK, Smith PD, Wang L, Thibodeau SN, et al. BRAF V600E Disrupts AZD6244-Induced Abrogation of Negative Feedback Pathways between Extracellular Signal-Regulated Kinase and Raf Proteins. Cancer Res. 2008;68:6145–53.

49. Chaikuad A, Tacconi EMC, Zimmer J, Liang Y, Gray NS, Tarsounas M, et al. A unique inhibitor binding site in ERK1/2 is associated with slow binding kinetics. Nat Chem Biol. 2014;10:853–60.

50. Xue Y, Martelotto L, Baslan T, Vides A, Solomon M, Mai TT, et al. An approach to suppress the evolution of resistance in $BRAF^{V600E}$-mutant cancer. Nature Medicine. 2017;23:929.

51. Cortez GS, Joseph S, Mclean JA, Mcmillen WT, Rodriguez MJ, Zhao G. Thieno[2,3-C]pyrrol-4-One Derivatives as Erk Inhibitors [Internet]. 2016 [cited 2019 Oct 29]. Available from: https://patentscope.wipo.int/search/en/detail.jsf?docId=WO2016106029

Figure 1. ERK1/2 inhibitors display distinct binding modes which influence their ability to modulate ERK1/2 phosphorylation. (**A**) The chemical structures and biochemical activity of the ERK1/2 inhibitors (ERKi) utilised in this study. ERK2 IC_{50} values were generated using a time-resolved fluorescence (TRF) assay. Proliferation IC_{50} values (96-hour Alamar Blue Cell viability assay) and pRSK IC_{50} values (4-hour MSD analysis) were performed in A375 cells. (**B**) X-ray crystal structures of ERK2 bound to each inhibitor. The binding mode of catERKi (GDC-094, pdb: 5k4i; BVD-523, pdb: 6gdq and LY-3214996, pdb: 6rq4) shows the Tyr36 conformation is "out" and its pi-pi interaction with Tyr64 is exemplified. The lower structures show Tyr36 bending into the ATP pocket interacting with the dmERKi that also extend further in the space left by the P-loop residue movement (Compound 27, pdb:6g9n and SCH772984, pdb: 6gdm). (**C**) COLO205, A375, HCT116 and Capan-1 cells were treated with the indicated concentrations of ERKi or MEKi (trametinib & selumetinib) for 2 hours prior to cell lysis and immunoblotting with the indicated antibodies. Mean normalized blot quantification is shown ± SEM, n = 3. Representative Western Blots are shown in Fig. S1-2. (**D**) *In vivo* pharmacodynamic effects following a single oral 50 mg/kg dose of compound 27 or 150 mg/kg dose of GDC-0994 to mice bearing subcutaneous COLO205 tumour xenografts.

Figure 2. When utilised at normalised concentrations dual-mechanism and catalytic ERKi delay pathway rebound as effectively as 'feedback buster' MEKi. HCT116 (**A-B**) cells were treated with the indicated normalized concentrations of ERKi (Compound 27, SCH772984, GDC-0994, BVD-523 & LY-3214996) or MEKi (trametinib & selumetinib) for 0.5-96 hours, prior to cell lysis and immunoblotting with the indicated antibodies. Representative Western Blots (**A**) and mean normalized blot quantification (**B**) are shown ± SEM, n = 3. Representative Western Blots for additional compounds are shown in Fig. S4. (**C-D**) HCT116 cells were treated with the indicated concentrations of ERKi or MEKi (trametinib, selumetinib & PD184352) for 2-72 hours, then fixed and permeabilized for staining with p-RSK (**C**) or p-ERK1/2 (**D**) antibodies before analysis using high content microscopy (HCM). Results are the mean of four independent experiments normalised to the DMSO control conditions.

Figure 3. Catalytic ERKi induce the nuclear accumulation of p-ERK1/2. (**A-B**) HCT116 cells were treated with normalised concentrations (Table S2) of the indicated ERKi or MEKi for 0-24 hours, then fixed and permeabilized for immunofluorescence with p-ERK1/2 or total ERK1/2 antibodies before analysis using high content microscopy (HCM). (**A**) Representative images, scale bar 10µM. (**B**) Mean signal per cell or the nuclear:cytoplasmic (N:C) ratio are shown. Normalised mean ± SEM, n = 3. *P < 0.05, ****P<0.0001 using two-way ANOVA and Dunnett's post hoc test, comparing each compound with DMSO treatment. (**C**) RT-qPCR analysis of the indicated transcripts following the treatment of HCT116, COLO205, A375 and Capan-1 cells with normalised concentrations of ERKi or MEKi for 24 hours. Data presented as Log_2 fold change values relative to DMSO (Mean ± SEM, n = 3). (**D-G**) HCT116 cells were treated with ERKi or MEKi for 0-24 hours, followed by compound withdrawal for up to 4 hours. (**D-E**) Cells were then fixed and permeabilized for immunofluorescence with p-ERK1/2 and total ERK1/2 antibodies before analysis by HCM (Mean ± SEM, n = 3). (**F-G**) Cells were then lysed and immunoblotted with the indicated antibodies. Representative Western Blots (**F**) and mean normalized blot quantification are shown, ± SEM, n = 3 (**G**). Representative Western Blots for additional compounds are shown in Fig. S8A.

Figure 4. The dual-mechanism ERKi SCH772984 induces a greater modulation of ERK1/2-dependent gene expression than the catalytic ERKi GDC-0994. HCT116, COLO205 and A375 cells were treated with DMSO, SCH772984 (200nM, 80nM and 200nM respectively) or GDC-0994 (5μM, 750nM and 750nM respectively) for 24h (~5x EC_{50} values – Table S3). RNA was extracted and gene expression profiling was performed using microarrays. (**A**) Heatmaps showing expression changes in a panel of 10 established ERK1/2 target genes. (**B**) Venn diagrams showing overlap of significantly up- or downregulated genes specific to either SCH772984 or GDC-0994 or commonly regulated by both ERKi. (**C**) The 10 most significant gene ontology (GO) terms from the common or SCH772984-specific downregulated gene signatures. (**D**) The 10 most significant GO terms from the common or SCH772984-specific upregulated gene signatures in HCT116 cells. (**E**) SCH772984-specific upregulated genes within the "response to type I interferon" GO term. Genes highlighted red have been shown to be transcriptionally repressed by ERK2 binding (39). (**F**) RT-qPCR analysis of the indicated transcripts following treatment of HCT116 cells with ERKi or MEKi for 24 hours. Compound concentrations were normalised as ~5x EC_{50} values from a 96h proliferation assay: Compound 27 (200nM), SCH772984 (200nM), GDC-0994 (5μM), BVD-523 (600nM), LY-3214996 (2μM), trametinib (45nM) & selumetinib (3μM). Data presented as Log_2 fold change values relative to DMSO. Mean values ± SD are shown, n = 3. *P<0.05, **P<0.01, ***P<0.001, ****P<0.0001 using one-way ANOVA and Tukey's post hoc test, comparing each compound with SCH772984 treatment. Microarray data are available in the ArrayExpress database (http://www.ebi.ac.uk/arrayexpress) under accession number E-MTAB-7959.

Figure 5. The anti-proliferative effects of ERKi correlate with their ability to inhibit ERK1/2 catalytic activity. (**A**) COLO205 and HCT116 cells were treated with the indicated concentrations of ERKi or MEKi for 24h, with a pulse of 10μM EdU for the final hour. Cells were then fixed and permeabilized for EdU detection and immunofluorescence with p-RSK or p-ERK1/2 and total ERK1/2 specific antibodies before analysis using high content fluorescence microscopy (Mean ± SEM, n = 3). (**B**) Table of the GI_{50} values for the indicated compounds in a panel of BRAF or KRAS mutant colorectal cancer (CRC) cell lines. GI_{50} values were interpolated from the EdU incorporation data shown in (**A**) or from the equivalent data sets shown in Fig. S9-10. (**C**) Mean GI_{50} values for the BRAF or KRAS mutant CRC cell lines. (**D**) Correlations between p-RSK levels and EdU incorporation following 24h treatment with the indicated ERKi or MEKi in CRC cell lines. Data interpolated from the sigmoidal non-linear regressions fitted to mean p-RSK and EdU incorporation data shown in (**A**) and Fig. S9-S10.

Figure 6. Acquired resistance to ERKi treatment involves restoration of ERK1/2 pathway activity in the presence of drug. (**A**) HCT116 cells were cultured in the presence of DMSO (Parental), 0.3µM Compound 27, 0.3µM SCH772984, 10µM GDC-0994, 1µM BVD-523, 3µM LY-3214996 or 3µM PD184352 for the indicated times and the number of cumulative doublings recorded. (**B**) HCT116 parental or cells that had been cultured continuously in the indicated compound for >115 days were washed and treated with the indicated compound concentrations for 24h, with a pulse of 10µM EdU for the final hour. Cells were then fixed and permeabilized for EdU detection, before analysis using high content fluorescence microscopy Normalised mean values ± SEM are shown, n = 4. (**C-D**) HCT116 parental or cell lines that have acquired resistance to the indicated compounds were incubated in the presence (+) or absence (-) of the indicated compounds for 24h. Cells were then lysed and immunoblotted with the indicated antibodies. Representative Western Blots (**C**) and mean normalized blot quantification (± SEM, n = 3) are shown (**D**).

Figure 1

A

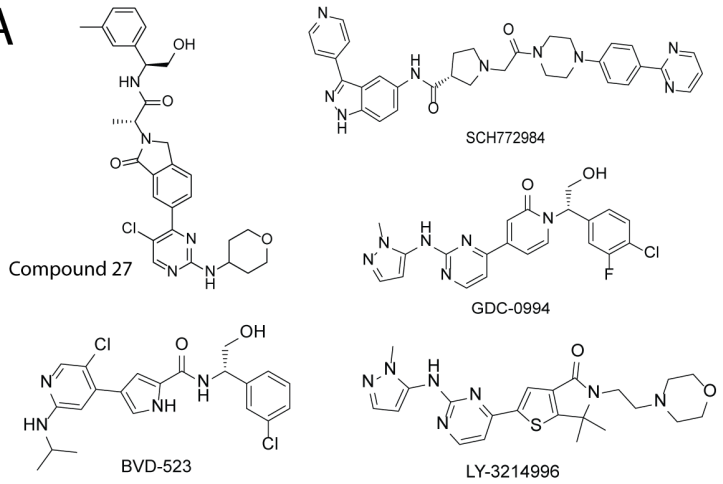

ERK1/2 inhibitor	ERK2 IC_{50} / nM	A375 proliferation IC_{50} / nM	pRSK IC_{50} / nM
Compound 27	3	4.9	2.4
SCH772984	1.2	37	10
GDC-0994	3.6	130	85
BVD-523	2.3	150	160
LY-3214996	68% at 3nM	350	340

B

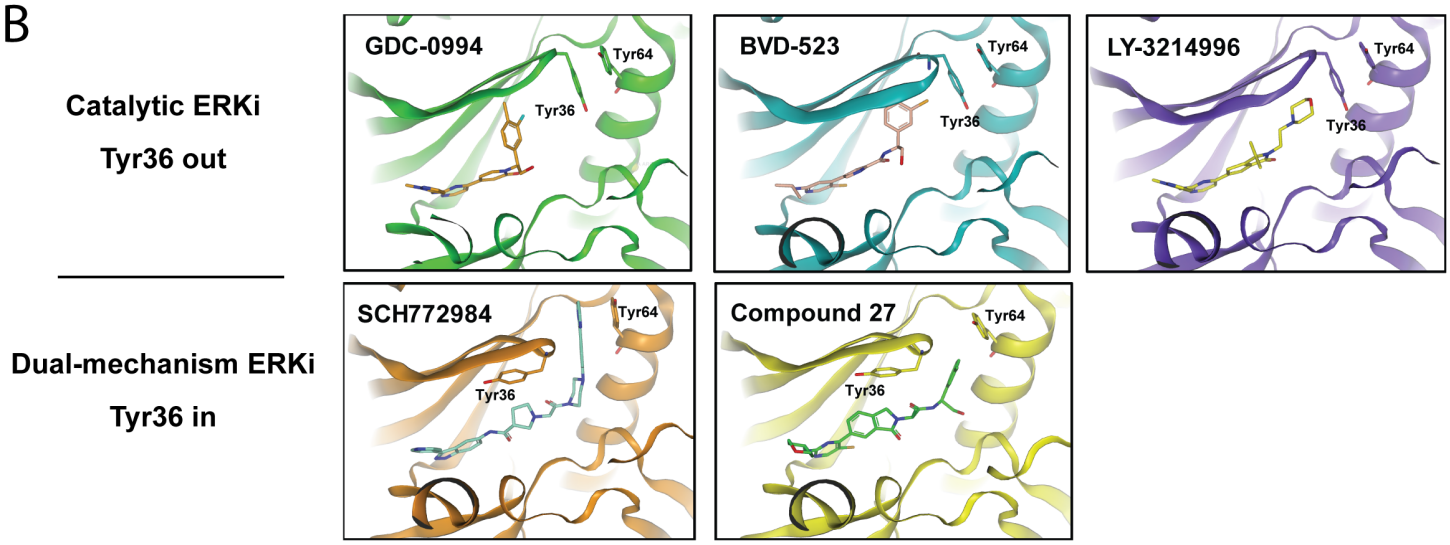

C

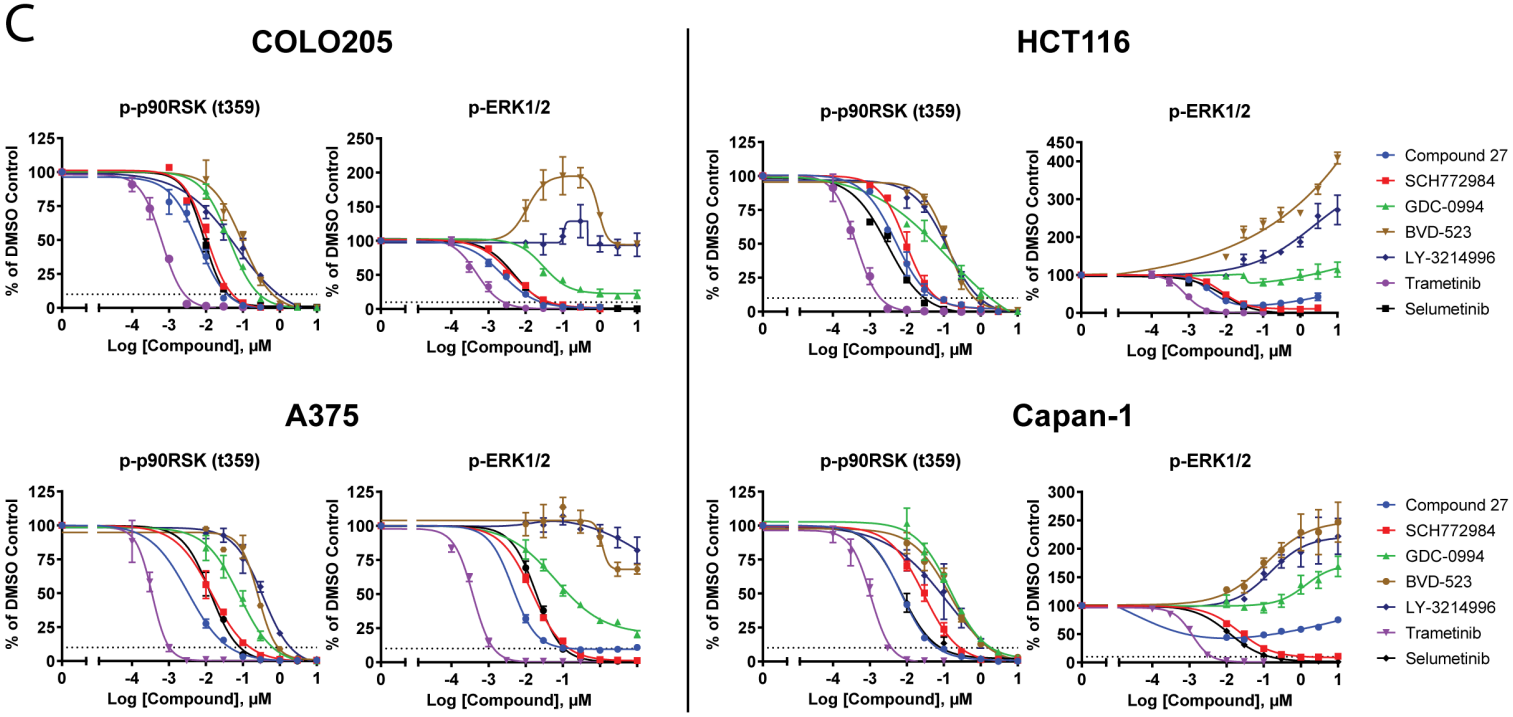

D

Figure 2

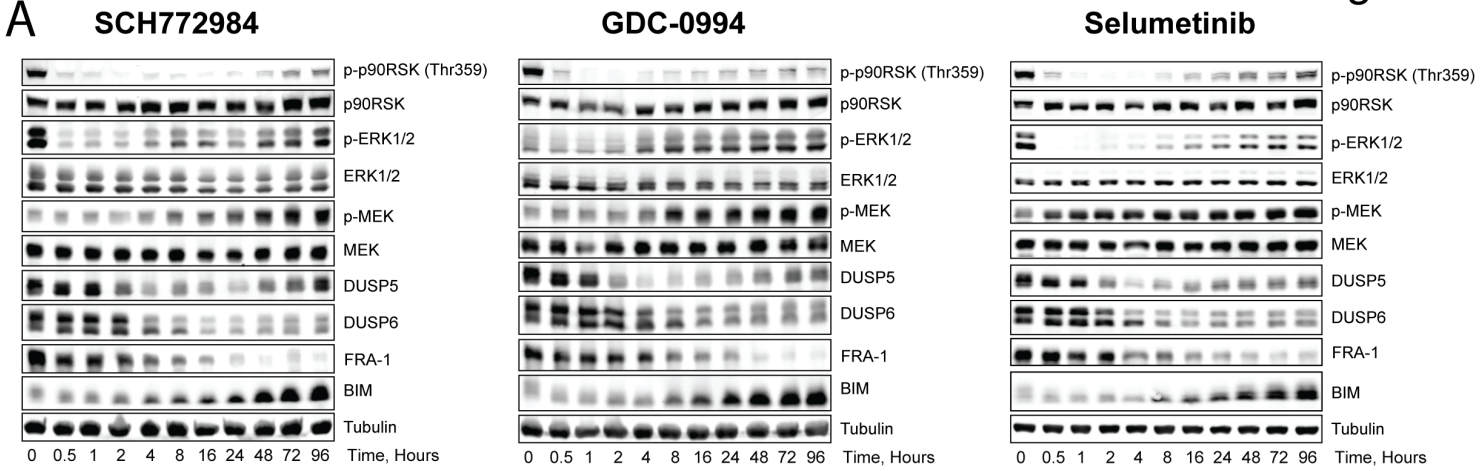

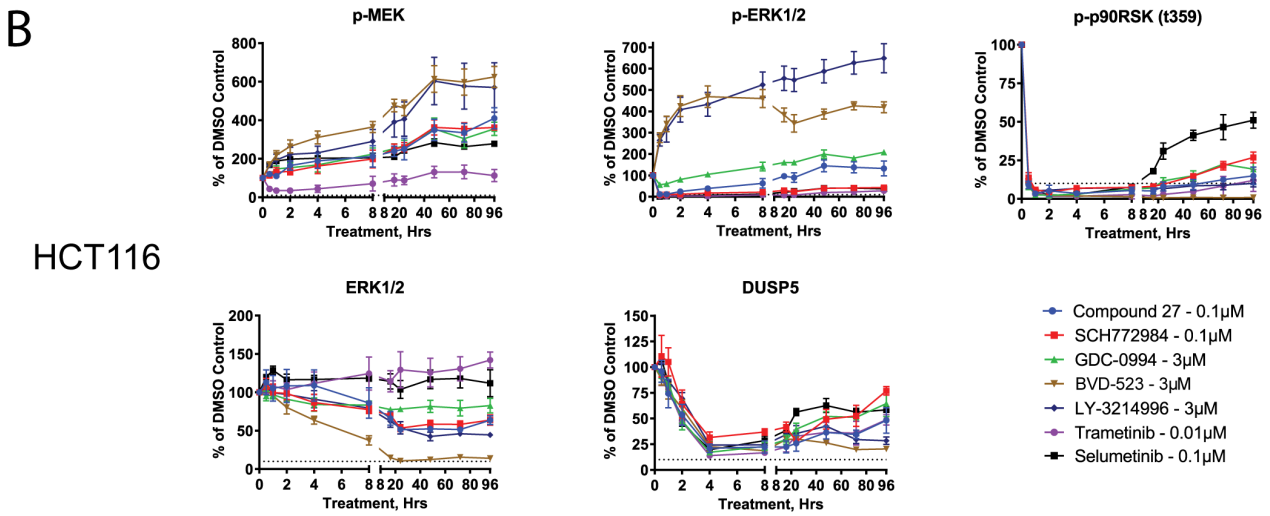

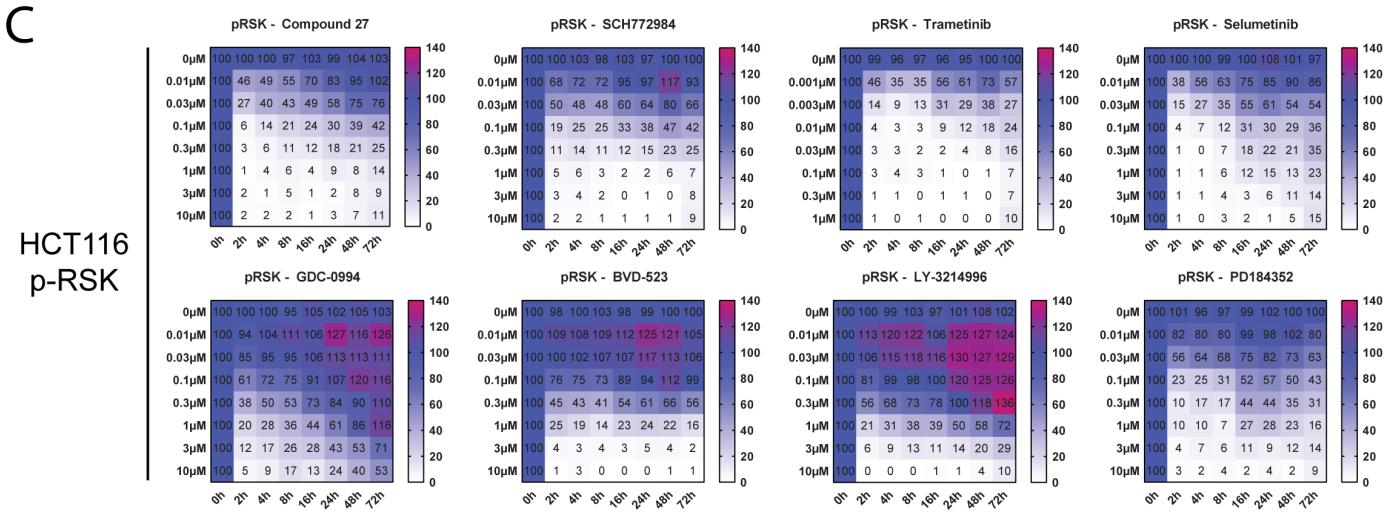

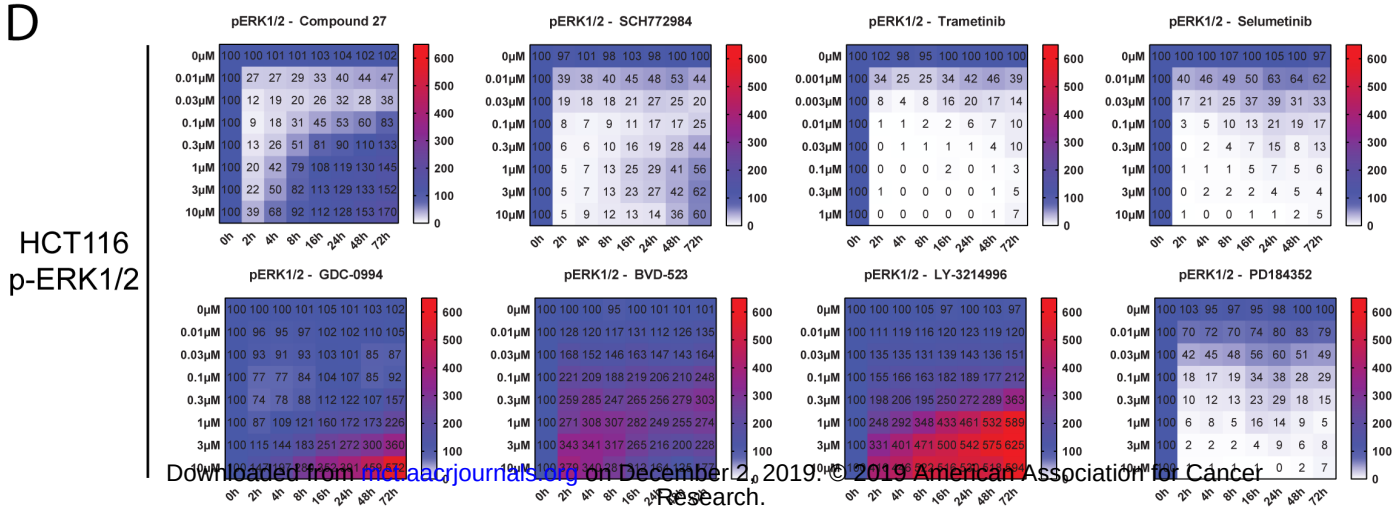

Figure 3

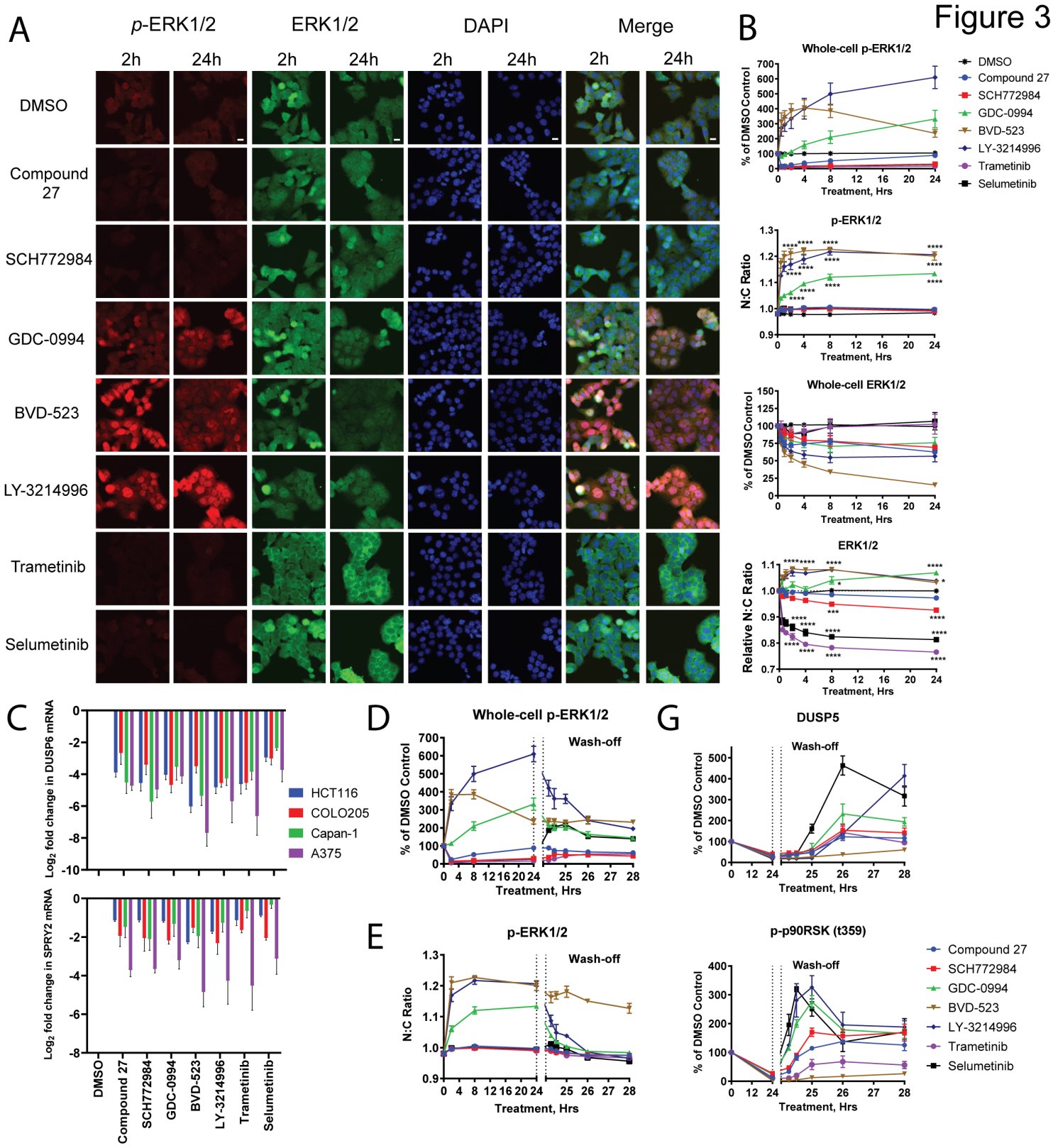

Figure 4

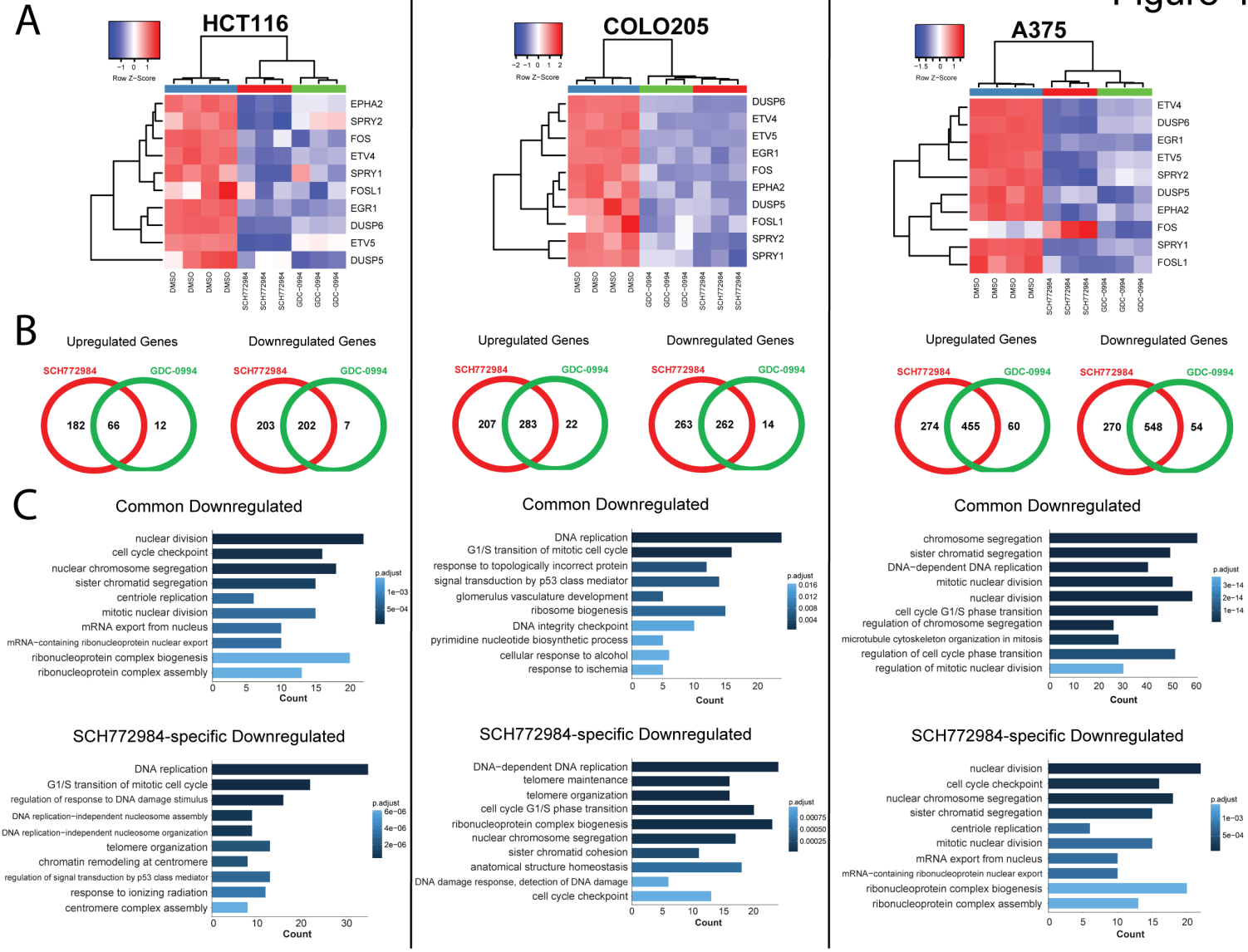

Figure 5

A

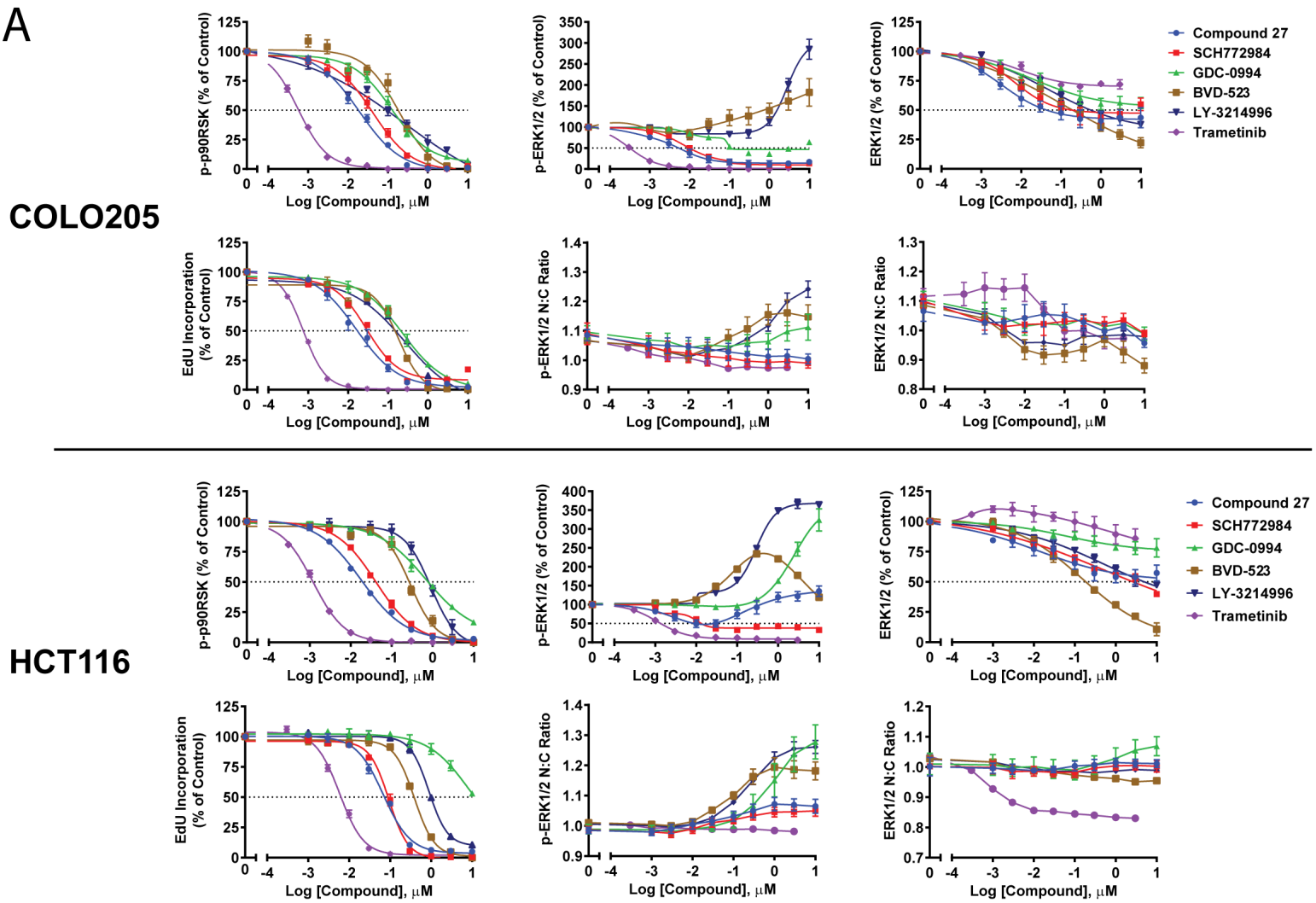

B

Indication	Cell line	Compound 27 GI_{50} (nM)	SCH772984 GI_{50} (nM)	GDC-0994 GI_{50} (nM)	BvD-523 GI_{50} (nM)	LY-3214996 GI_{50} (nM)	Trametinib GI_{50} (nM)
BRAF CRC	CO115	67	91	2,890	258	581	2.04
	COLO205	18	37	249	150	154	0.75
	HT29	23	88	635	210	295	1.04
	RKO	165	106	>10,000ǂ	1,253ǂ	>10,000ǂ	13.45
KRAS CRC	DLD-1	615	551	14,552*	772	2,688	19.85
	HCT116	71	88	11,589*	384	992	6.34
	LoVo	106	89	>10,000ǂ	252	721	8.41
	Sw480	71	219	8,067	272	527	4.31

C

Mean GI_{50} values

Indication	Compound 27 GI_{50} (nM)	SCH772984 GI_{50} (nM)	GDC-0994 GI_{50} (nM)	BvD-523 GI_{50} (nM)	LY-3214996 GI_{50} (nM)	Trametinib GI_{50} (nM)
BRAF CRC	68.25	80.5	1,258	206	343.3	4.32
KRAS CRC	215.75	236.75	11,403	420	1,232	9.73
KRAS GI_{50} / BRAF GI_{50}	**3.16**	**2.94**	**9.06**	**2.04**	**3.59**	**2.25**

D

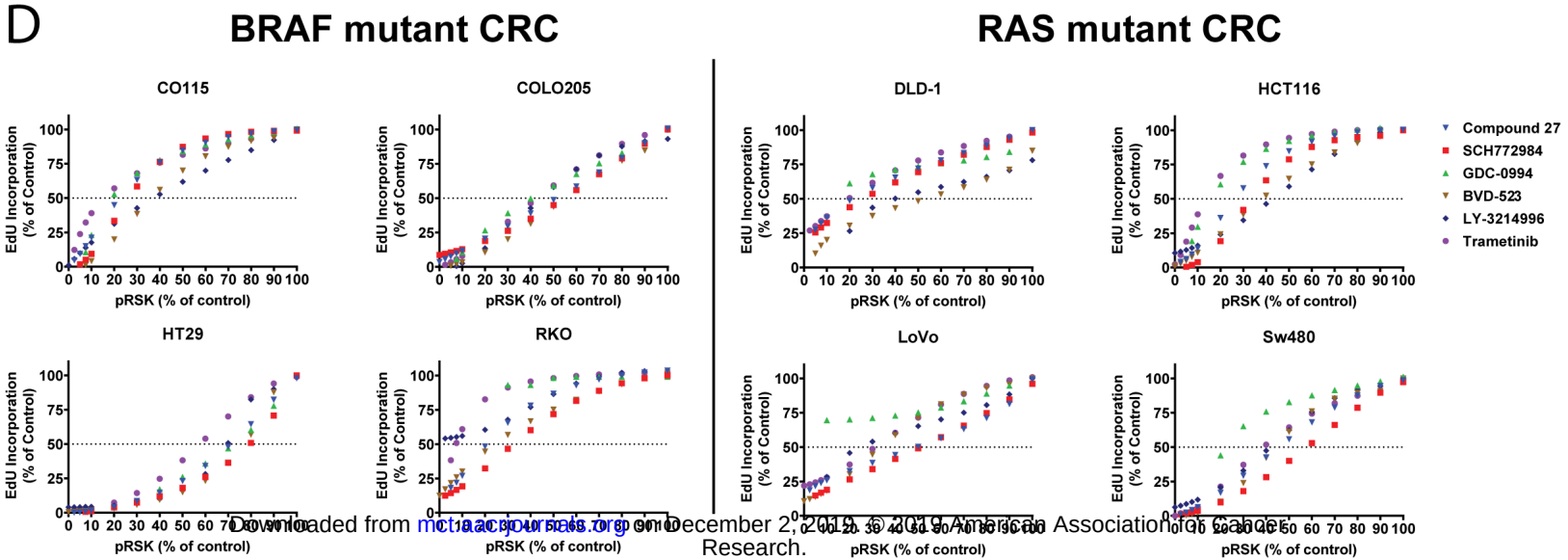

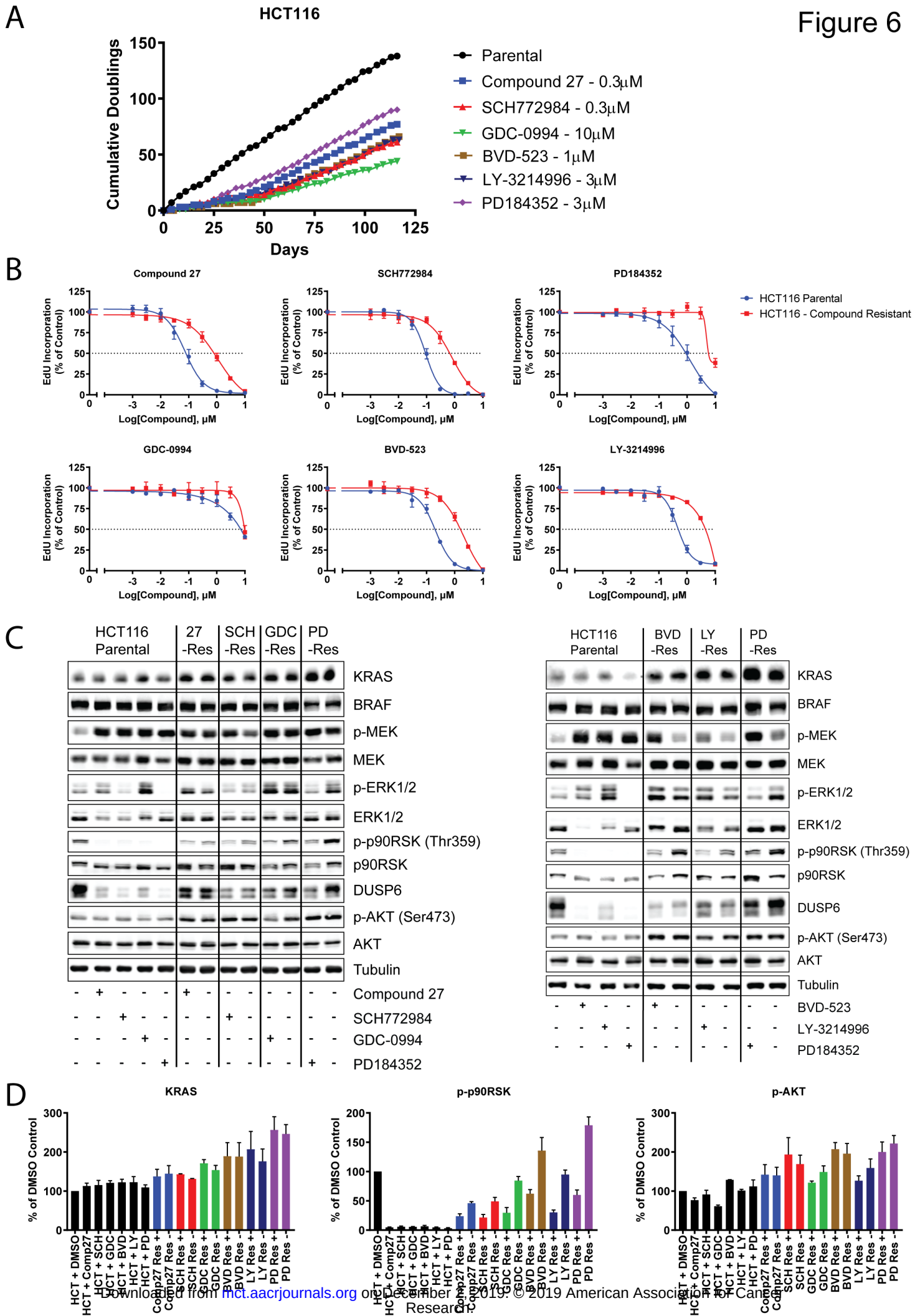

AACR American Association for Cancer Research

Molecular Cancer Therapeutics

Dual-mechanism ERK1/2 inhibitors exploit a distinct binding mode to block phosphorylation and nuclear accumulation of ERK1/2

Andrew M Kidger, Joanne M Munck, Harpreet K Saini, et al.

Mol Cancer Ther Published OnlineFirst November 20, 2019.